J Low Temp Phys (2010) 158: 105–111
DOI 10.1007/s10909-009-9934-7

Absorption Spectrum of Na Atoms Attached to Helium Nanodroplets

A. Hernando · M. Barranco · R. Mayol · M. Pi · F. Ancilotto · O. Bünermann · F. Stienkemeier

Received: 11 June 2009 / Accepted: 30 July 2009 / Published online: 11 August 2009

Abstract We present an analysis of the electronic $3p \leftarrow 3s$ excitation of Na atoms attached to ^{3}He and ^{4}He droplets. Once the ground state structure of the doped drops has been obtained within finite-range density functional theory, we determine the time-correlation function of the Na atom evolving in the full three-dimensional $^2\Pi_{1/2}$, $^2\Pi_{3/2}$ and $^2\Sigma_{1/2}$ potentials generated by its pairwise interaction with the helium atoms. The Fourier analysis of the time-correlation function determines the absorption spectrum of Na, which is compared with the experimental spectrum. We show that the existence of a redshifted shoulder in the absorption line of Na@^{4}He$_N$, absent in Na@^{3}He$_N$, is due to the wider vibrational motion of the dopant atom in the dimple it causes on the surface of the droplet.

Keywords Helium droplets · Impurity absorption spectrum

PACS 36.40.-c · 33.20.Kf · 67.40.Yv · 71.15.Mb

Supported in part by Grant No. FIS2008-00421/FIS from DGI, Spain (FEDER).

A. Hernando (✉) · M. Barranco · R. Mayol · M. Pi
Departament ECM, Facultat de Física, and IN²UB, Universitat de Barcelona, Diagonal 647, 08028 Barcelona, Spain
e-mail: alberto@ecm.ub.es

F. Ancilotto
INFM-DEMOCRITOS and Dipartimento di Fisica 'G. Galilei', Università di Padova, via Marzolo 8, 35131 Padova, Italy

O. Bünermann · F. Stienkemeier
Physikalisches Institut, Universität Freiburg, Hermann-Herder-St. 3, 76104 Freiburg, Germany

1 Introduction

It is well established that superfluid droplets made of ^{4}He atoms provide an ideal matrix for spectroscopic studies at temperatures of 0.38 K [1, 2]. Droplets made of ^{3}He atoms are colder (0.15 K), but normal fluid [3]; the possibility to compare both systems gives valuable insight into the quantum nature of Bose and Fermi drops [4].

Electronic spectroscopy is a powerful tool to reveal the structure of embedded impurities, see e.g. [5–9] and references therein. Indeed, the shift and width of the electronic transitions are key observables to determine the position of an atomic impurity in a helium drop. Whereas almost all impurities are solvated, alkali atoms are weakly bound to helium droplets and reside in dimples on the drop surface, irrespective of the isotope. Several experimental and theoretical works have been able to describe many features of the absorption spectrum of alkali atoms on helium droplets [10–17].

Density functional (DF) theory has naturally lent itself to the study of these complexes, since the large size of the experimental drops, made of several thousand atoms, still prevents the use of more microscopic approaches [18]. All theoretical methods are applied in conjunction with some approximations, like the diatomics-in-molecules assumption, the Franck-Condon principle and an atomic pairwise approximation for the drop-impurity interaction. We refer the reader e.g., to [10, 19] for a thorough description of the Path Integral Monte Carlo and DF approaches to this problem.

To determine the absorption line shape, instead of carrying out the much demanding Fourier transform of the time-correlation function of the dopant atom moving in the potential energy surfaces (PES), obtained from the helium-excited impurity potentials, it is customary to carry out a semiclassical average on the states accessible from the ground state by a dipole excitation. While it is justified in most cases, this semiclassical average washes out details of the absorption spectrum, hampering a deeper understanding of some features that appear in the spectrum and may distinguish the ^{4}He from the ^{3}He droplet situation.

In this work we discuss one such feature, namely the redshifted shoulder in the absorption line of Na@^{4}He$_N$ that does not show up in Na@^{3}He$_N$. The origin of this shoulder was correctly anticipated in [17]; we explicitly show here that it is due to the vibrational motion of the Na atom in the dimple. These vibrations are wider in ^{4}He than in ^{3}He droplets because of the less pronounced dimple in the former than in the latter, yielding more intense bound-bound transitions in ^{4}He than in ^{3}He drops.

2 Method

Our theoretical analysis has been carried out using the functional $\mathcal{E}$ of [20] for ^{4}He, and of [21] for ^{3}He, together with the Na-He $X^2\Sigma$ potential of [22] for the ground state, and the $^2\Pi$ and $^2\Sigma$ potentials of [23] for the excited states. The energy of the Na-helium system is written as a functional of the Na wave function $\Psi^{gs}(\mathbf{r})$ and the helium atomic density $\rho(\mathbf{r})$. To handle the large number of ^{3}He atoms involved in current experiments, we have used a Thomas-Fermi approximation to express the

kinetic energy density as a function of $\rho(\mathbf{r})$ and its gradient [15, 16]. Within the pair potential approximation, we write the energy of the system as

$$E = \int d\mathbf{r}\mathcal{E}[\rho(\mathbf{r})] + \frac{\hbar^2}{2m_{Na}} \int d\mathbf{r}|\nabla\Psi^{gs}(\mathbf{r})|^2 + \int\int d\mathbf{r}\, d\mathbf{r}'|\Psi^{gs}(\mathbf{r})|^2 V_{X^2\Sigma}(|\mathbf{r}-\mathbf{r}'|)\rho(\mathbf{r}').$$

We have selfconsistently solved the equations that result from the variations of E with respect to Ψ^{gs} and $\rho(\mathbf{r})$, see [19] for the details.

Once the helium density and impurity wave function have been determined, we have obtained the absorption spectrum around the $3p \leftarrow 3s$ transition using two different approaches with the aim of comparing their results and determine the origin of the redshifted shoulder. Using the Born-Oppenheimer approximation to factorize the electronic and nuclear wave functions, and the Franck-Condon approximation by which the positions of the atomic nuclei are kept frozen during the transition, the line shape for an electronic transition from the ground state (gs) to the excited state (ex) can be calculated as the Fourier transform of the time-correlation function, namely [19]

$$I(\omega) \propto \sum_m \int dt e^{-i(\omega+\omega^{\rm gs})t} \int d^3\mathbf{r}\, \Psi^{\rm gs}(\mathbf{r})^* e^{(it/\hbar)H_m^{\rm ex}} \Psi^{\rm gs}(\mathbf{r}), \quad (1)$$

where $\hbar\omega^{\rm gs}$ is the eigenenergy of Na in its ground state. The Hamiltonian in the time evolution operator $e^{(it/\hbar)H_m^{\rm ex}}$ is defined as $H_m^{\rm ex} = T + V_m^{\rm ex}(\mathbf{r})$, where T is the kinetic energy operator and $V_m^{\rm ex}(\mathbf{r})$ is the PES defined by the mth eigenvalue of the excited potential matrix $V_T(\mathbf{r}) = U(\mathbf{r}) + V_{\rm SO}$, where $U(\mathbf{r})$ is the convolution of the excited pairpotentials $^2\Pi$ and $^2\Sigma$ with the helium density $\rho(\mathbf{r})$, and $V_{\rm SO}$ accounts for the spin-orbit coupling (see [19] for the details). Introducing in (1) $\Psi^{\rm gs}(\mathbf{r}) = \sum_\nu a_\nu^m \Psi_\nu^m(\mathbf{r})$, where $\Psi_\nu^m(\mathbf{r})$ are the eigenfunctions of $H_m^{\rm ex}$ and $a_\nu^m = \int d^3\mathbf{r}\Psi_\nu^m(\mathbf{r})^*\Psi^{\rm gs}(\mathbf{r})$ are the Franck-Condon factors, we obtain

$$I(\omega) \propto \sum_m \int dt e^{-i(\omega+\omega^{\rm gs})t} \sum_\nu |a_\nu^m|^2 e^{i\omega_\nu^m t} = \sum_m \sum_\nu |a_\nu^m|^2 \delta(\omega + \omega^{\rm gs} - \omega_\nu^m), \quad (2)$$

where $\hbar\omega_\nu^m$ are the eigenvalues of $H_m^{\rm ex}$.

If the Franck-Condon factors arise from the overlap between the gs and excited states with large quantum numbers, corresponding to the continuous or quasicontinuous spectrum of $H_m^{\rm ex}$, we can assume that $\langle T\rangle \ll \langle V_m^{\rm ex}\rangle$, and the Hamiltonian is approximated by $H_m^{\rm ex} \sim V_m^{\rm ex}(\mathbf{r})$. Introducing this approximation in (1) and integrating over time we get a semiclassical expression for $I(\omega)$

$$I(\omega) \propto \sum_m \int d^3\mathbf{r}\, |\Psi^{\rm gs}(\mathbf{r})|^2 \delta[\omega - (V_m^{\rm ex}(\mathbf{r})/\hbar - \omega^{\rm gs})]. \quad (3)$$

We have recently proposed a method [26] to evaluate this expression using an atomiclike, 'DF sampling' simulation, inspired by that proposed in [25]. The helium den-

sity, once determined by solving the variational DF equations, is stochastically represented by a large number of hard spheres configurations $n_c \sim 10^6$. This is done by importance sampling techniques [24] with $\rho_4(\mathbf{r})/N$ or $\rho_3(\mathbf{r})/N$ as probability density functions. As a result, for the $\{j\}$th configuration a set of N positions $\{\mathbf{r}_i^{\{j\}}\}_{i=1}^N$ is randomly generated. The position of the impurity $\mathbf{r}_{\mathrm{Na}}^{\{j\}}$ corresponding to the $\{j\}$th configuration is analogously generated using $|\Psi^{\mathrm{gs}}(\mathbf{r})|^2$ as probability density.

To simulate the effect of He-He correlations, the radius of the hard spheres $R_i^{\{j\}}$ is rescaled with the local value of the density

$$R_i^{\{j\}} = \frac{h}{2}\left(\frac{\rho_0}{\bar{\rho}(\mathbf{r}_i^{\{j\}})}\right)^{1/3}, \tag{4}$$

where $\bar{\rho}(\mathbf{r}_i^{\{j\}})$ is the coarse-grained He density obtained by smoothing the actual density within a spherical cavity of radius h (see [20, 21] for more details), and ρ_0 is the saturation density value. This scaling has no effect in the bulk of the droplet far from the impurity, but allows one to better take into account the density inhomogeneities around the impurity and/or in the surface region of the droplet. Introducing this correlation in the generation of the positions set by an acceptance-rejection method, we have checked that we accurately recover, when all the n_c configurations are considered, the DF helium density $\rho(\mathbf{r})$, as shown for example in Fig. 1 for the Na@^{4}He$_{1000}$ complex.

To determine the line shape, for each configuration $\{j\}$ we obtain the eigenvalues $V_m^{\mathrm{ex}}\{j\}$ of the excited-state energy matrix $\sum_i U(|\mathbf{r}_i^{\{j\}} - \mathbf{r}_{\mathrm{Na}}^{\{j\}}|) + V_{\mathrm{SO}}$ (Eq. (16) of [19]), and subtract from them the pairwise sum of the ground state pair-potential interactions $V^{\mathrm{gs}}\{j\} = \sum_i V_{X^2\Sigma}(|\mathbf{r}_i^{\{j\}} - \mathbf{r}_{\mathrm{Na}}^{\{j\}}|)$ to obtain the excitation energy. We divide the excitation energy interval into a large number of narrow bins and collect the frequency distribution of excitation energies (histogram). Finally, the frequency

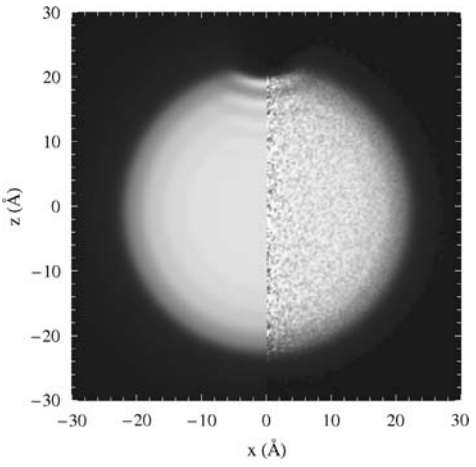

Fig. 1 Helium density corresponding to Na@^{4}He$_{1000}$ on a plane of symmetry of the complex. *Left region*: result of the DF calculation. *Right region*: atomiclike simulation. The lighter the grey, the higher the density

distribution is normalized dividing it by the number of configurations n_c, i.e.,

$$I(\omega) \propto \sum_m \frac{1}{n_c} \sum_{\{j\}}^{n_c} \delta[\omega - (V_m^{\rm ex}\{j\} - V^{\rm gs}\{j\})/\hbar]. \tag{5}$$

3 Results and Discussion

Figure 2 shows the absorption spectrum calculated using the semiclassical formula (5) compared with the experimental results [15, 16]. It can be seen that for both isotopes the locations of the D_1 and D_2 peaks arising from $^2\Pi_{1/2}, ^2\Pi_{3/2} \leftarrow X^2\Sigma_{1/2}$,respectively, are well reproduced; however, the widths are underestimated. This is in part a finite size effect, as can be seen comparing the results we have obtained for $N = 1000$ and 3000 (right panel of this figure). Our results are qualitatively similar to those of [10]. We want to mention that in the case of Ca, our DF sampling method yields the correct width of the absorption line [26].

Figure 3 shows the absorption spectrum calculated from the Fourier transform of the time-correlation function, (2). Notice that besides the bound-unbound transitions that contribute the most to the D_1 and D_2 peaks, there are a few narrow peaks to their left arising from bound-bound transitions. The transitions that arise from the $^2\Pi_{1/2}$ PES are very weak in the case of Na@^{3}He$_{1000}$ and much more pronounced for Na@^{4}He$_{1000}$. In both cases, those arising from the $^2\Pi_{3/2}$ PES are masked below the absorption peak and are not resolved experimentally, although they might be the reason of the more marked splitting of the line for ^{4}He than for ^{3}He, see Fig. 2. Since all ingredients in the calculation are the same for both isotopes but the equilibrium helium density, the redshifted shoulder has to be attributed to the dimple structure that is different for the two isotopes.

We have found that Na resides in a dimple that is deeper for ^{3}He than for ^{4}He droplets [15, 16]. Since the energy of the absorption peak is sensitive to the helium

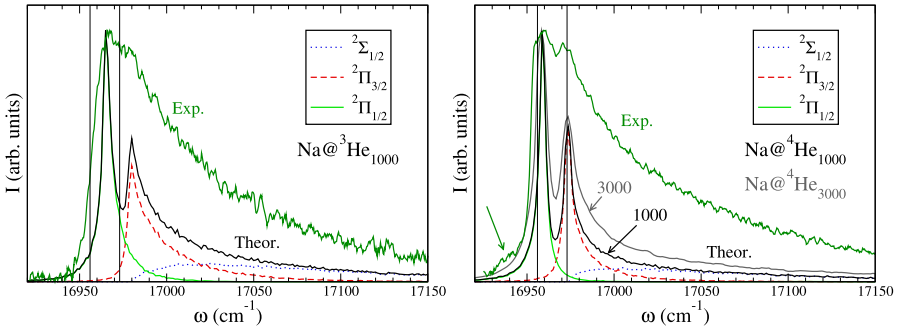

Fig. 2 (Color online) *Left panel*: Absorption spectrum (arbitrary units) for Na@^{3}He$_{1000}$. The experimental result, labeled as 'Exp.', corresponds to $N \sim 5000$. The theoretical result, labeled as 'Theor.', has been obtained using the semiclassical approach by adding the three components contributing to it and normalized so that the experimental and theoretical peaks have the same height. *The vertical thin lines* indicate the location of the absorption lines of the free Na atom. *Right panel*: same as left panel for Na@^{4}He$_N$ with $N = 1000$ and 3000. The redshifted shoulder is indicated by *an arrow*

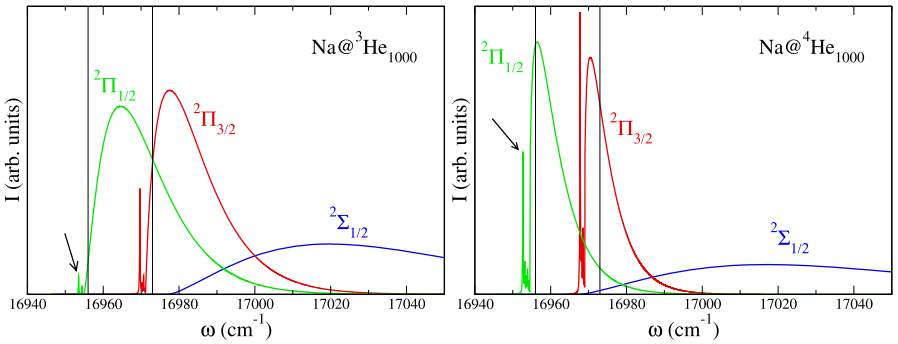

Fig. 3 (Color online) *Left panel*: Absorption spectrum (arbitrary units) for Na@^{3}He$_{1000}$ obtained using the Fourier transform of the time-correlation function. For the sake of clarity, we do not show the experimental peak nor add the three components, and the excitation energy range has been reduced with respect to that of Fig. 2. *Right panel*: same as left panel for Na@^{4}He$_{1000}$. The bound-bound transitions relevant for the discussion are indicated by an arrow. They are about an order of magnitude smaller for ^{3}He than for ^{4}He drops

amount around the dopant, a larger shift of this peak from that of the free Na atom peak is expected for ^{3}He than for ^{4}He drops. This is indeed what the experimental and theoretical results show in Figs. 2 and 3. The shallower dimple in the case of ^{4}He drops causes the appearance of the shoulder. A deeper dimple 'constrains' the lateral motion of the impurity in the $X^2\Sigma_{1/2}$ potential well and may reduce the number and/or intensity of bound-bound transitions that contribute to the absorption peak. For that reason, these lines show up for ^{4}He and not for ^{3}He droplets, semi-quantitatively explaining the features of the experimental absorption line of Na.

4 Summary

We have studied the dipole absorption line of Na atoms attached to helium droplets using a full three dimensional approach and the Fourier analysis of the time-correlation function of the impurity. This has allowed us to identify the main features of the absorption spectrum for both the ^{4}He and ^{3}He cases, and ascertain the origin of the redshifted shoulder that appears in the experimental line of Na@^{4}He$_N$.

We have also discussed in some detail a DF sampling simulation of the absorption line that can be straightforwardly applied to describe the line shape instead of the cumbersome procedure of coupling the dipole excitation with the surface fluctuations of the helium moiety around the dopant [27].

References

1. R. Fröchtenicht, J.P. Toennies, A. Vilesov, Chem. Phys. Lett. **229**, 1 (1994)
2. M. Hartmann, R.E. Miller, J.P. Toennies, A. Vilesov, Phys. Rev. Lett. **75**, 1566 (1995)
3. J. Harms, M. Hartmann, J.P. Toennies, A.F. Vilesov, B. Sartakov, J. Mol. Spectrosc. **185**, 204 (1997)
4. M. Hartmann, F. Mielke, J.P. Toennies, A.F. Vilesov, Phys. Rev. Lett. **76**, 4560 (1996)

5. J.P. Toennies, A.F. Vilesov, Angew. Chem. Int. Ed. **43**, 2622 (2004)
6. F. Stienkemeier, K.K. Lehmann, J. Phys. B **39**, R127 (2006)
7. J. Tiggesbäumker, F. Stienkemeier, Phys. Chem. Chem. Phys. **9**, 4748 (2006)
8. M.Y. Choi, G.E. Douberly, T.M. Falconer, W.K. Lewis, C.M. Lindsay, J.M. Merrit, P.L. Stiles, R.E. Miller, Int. Rev. Phys. Chem. **25**, 15 (2006)
9. K. Szalewicz, Int. Rev. Phys. Chem. **27**, 273 (2008)
10. A. Nakayama, K. Yamashita, J. Chem. Phys. **114**, 780 (2001)
11. F. Ancilotto, E. Cheng, M.W. Cole, F. Toigo, Z. Phys. B **98**, 323 (1995)
12. F. Stienkemeier, J. Higgins, C. Callegari, S.I. Kanorsky, W.E. Ernst, G. Scoles, Z. Phys. D **38**, 253 (1996)
13. F.R. Brühl, R.A. Trasca, W.E. Ernst, J. Chem. Phys. **115**, 10220 (2001)
14. O. Bünermann, M. Mudrich, M. Weidemüller, F. Stienkemeier, J. Chem. Phys. **121**, 8880 (2004)
15. F. Stienkemeier, O. Bünermann, R. Mayol, F. Ancilotto, M. Barranco, M. Pi, Phys. Rev. B **70**, 214509 (2004)
16. R. Mayol, F. Ancilotto, M. Barranco, M. Pi, O. Bünermann, F. Stienkemeier, J. Low Temp. Phys. **138**, 229 (2005)
17. O. Bünermann, G. Droppelmann, A. Hernando, R. Mayol, F. Stienkemeier, J. Phys. Chem. A **111**, 12684 (2007)
18. M. Barranco, R. Guardiola, S. Hernández, R. Mayol, M. Pi, J. Low Temp. Phys. **142**, 1 (2006)
19. A. Hernando, M. Barranco, R. Mayol, M. Pi, M. Krośnicki, Phys. Rev. B **77**, 024513 (2008)
20. F. Dalfovo, A. Lastri, L. Pricaupenko, S. Stringari, J. Treiner, Phys. Rev. B **52**, 1193 (1995)
21. M. Barranco, M. Guilleumas, E.S. Hernández, R. Mayol, M. Pi, L. Szybisz, J. Low Temp. Phys. **136**, 139 (2004)
22. S.H. Patil, J. Chem. Phys. **94**, 8089 (1991)
23. J. Pascale, Phys. Rev. A **28**, 632 (1983)
24. F. Salvat, J.M. Fernández, J. Senpau, *Penelope-2008: A Code System for Monte Carlo Simulation of Coupled Electron-Photon Transport*, OECD Nuclear Energy Agency, Issy-les-Moulineaux, France (2009). Available in pdf format at http://www.nea.fr/html/dbprog/peneloperef.html
25. T. Nakatsukasa, K. Yabana, G.F. Bertsch, Phys. Rev. A **65**, 032512 (2002)
26. O. Bünermann, M. Dvorak, F. Stienkemeier, A. Hernando, R. Mayol, M. Pi, M. Barranco, F. Ancilotto, Phys. Rev. B **79**, 214511 (2009)
27. A. Hernando, M. Barranco, R. Mayol, M. Pi, F. Ancilotto, Phys. Rev. B **78**, 184515 (2008)